ELSEVIER

Diamond and Related Materials 8 (1999) 1277–1284

DIAMOND AND RELATED MATERIALS

Plasma dynamics inferred from optical emission spectra, during diamond-like thin film pulsed laser deposition

R. Diamant [a,*], E. Jimenez [b], E. Haro-Poniatowski [a], L. Ponce [b], M. Fernandez-Guasti [a], J.C. Alonso [c]

[a] *Universidad Autonoma Metropolitana, Dpto. de Fisica, Iztapalapa, A.P. 55-534, México D.F. 09340, Mexico*
[b] *IMRE-Universidad de la Habana Vedado 10400, C. Habana, Cuba*
[c] *Instituto de Investigaciones en Materiales, UNAM, A.P. 70-360, México D.F. 09340, Mexico*

Received 30 October 1998; received in revised form 8 February 1999; accepted 15 February 1999

Abstract

Diamond-like thin films were produced via PLD with the fundamental line of a Nd:YAG laser, while the plasma dynamics were studied non-destructively by emission spectroscopy. Spectra obtained by analysing the plasma optical emission at various distances from the ablated graphite surface show how the composition and temperature vary within the plasma plume. The collected data allow the identification of various emitting species at different regions of the expanding plasma and estimation of their velocities. The further ahead in the plume, the more the ablated material is ionised. Temperatures are determined from the continuous broad background, while the plasma cools as it expands. The influence of substrate temperature on the resulting film structure is also studied through Raman scattering measurements. Optical microscope pictures are taken to evaluate surface quality. Plasma ionisation degree and kinetic energies are enough to grow diamond-like films, but high substrate temperatures favour graphitic order.

Keywords: Pulsed laser deposition; Emission spectroscopy; Raman spectroscopy

1. Introduction

Synthesis of diamond-like films is a front-line research area at this time owing to its important potential applications. Diamond is a form of carbon with a special combination of physical and chemical properties that cannot be realised in other materials [1]. Among these, the important ones are hardness, wear resistance, chemical inertness, high electrical resistivity, optical transparency, high thermal conductivity.

Recently, pulsed laser deposition (PLD) has been used to deposit a wide variety of materials basically for the following reasons: almost any material can be ablated, complicated stoichiometries can be controlled to a great extent, very high kinetic energies of the ablated species are attained together with high instantaneous deposition rates [2]. High kinetic energies, ionisation degree and instantaneous deposition rates seem to favour the formation of sp^3 carbon bonds on the film when ablating a graphite target. This type of bonding is held responsible for the diamond-like features in the resulting films [3–9].

Although we know which factors favour the formation of sp^3 bonds, the exact mechanisms that lead to the film structure are not very well understood yet. A better knowledge of the plasma dynamics and its composition must help us to answer related questions and possibly to control further the resulting structure and to enhance particular film properties.

The convenient laser energy densities to grow high quality films usually result in plasma ignition and a bright plume extending up to several centimetres from the target [10]. Optical emission spectroscopy is an excellent and non-destructive way to examine PLD ablation plumes. In general, the whole optical emission is linearly related to the amount of material ablated, although a great amount of the plasma atoms and molecules are in the ground state or decay through non-radiative processes. After the laser pulse, the emission of most of the observed atomic and molecular transitions are present for much longer times than their correspond-

* Corresponding author. Fax: +52-5-7-24-46-11.
E-mail address: ruth@xanum.uam.mx (R. Diamant)

0925-9635/99/$ – see front matter
PII: S0925-9635(99)00112-0

ing lifetimes, this is due to re-excitation within the plasma plume [10]. Plasma optical emission can be monitored in real time without disturbing deposition conditions.

In the first part of this work we characterise, by means of optical emission spectroscopy, the Nd:YAG laser ($\lambda = 1064$ nm) induced carbon plasma as it expands into vacuum, before reaching and condensing on the substrate. Similar studies have been done recently, ablating a graphite target with excimer lasers [7,8]. With shorter laser wavelengths, lower output intensity is needed to create favourable conditions for diamond-like film growth. However, not only the laser intensity for a given wavelength, also the wavelength alone leads to different film properties [3–9], although this effect is not well understood yet. Laser wavelength must be then an important parameter in the plasma formation and dynamics. In our work, we study the outcome using an infrared laser source. Initially, time-integrated but spatially and spectrally resolved information is acquired, allowing identification of emitting species and temperature calculations. Then, time-resolved measurements are performed in order to estimate velocities.

To complement plasma studies, the resulting film structure is investigated by means of Raman spectroscopy. Graphitic carbon and other sp^2-bonded amorphous carbons are strong Raman scatterers in spite of their intense optical absorption [11]. Likewise, diamond and related carbons have a strong Raman response. Raman spectra may provide a large amount of structural and phase information [5,9,11–13], but great care has to be taken in order to draw valid conclusions.

Substrate temperature is introduced as another independent experimental parameter because it also plays a significant role in the resulting film structure [5,12].

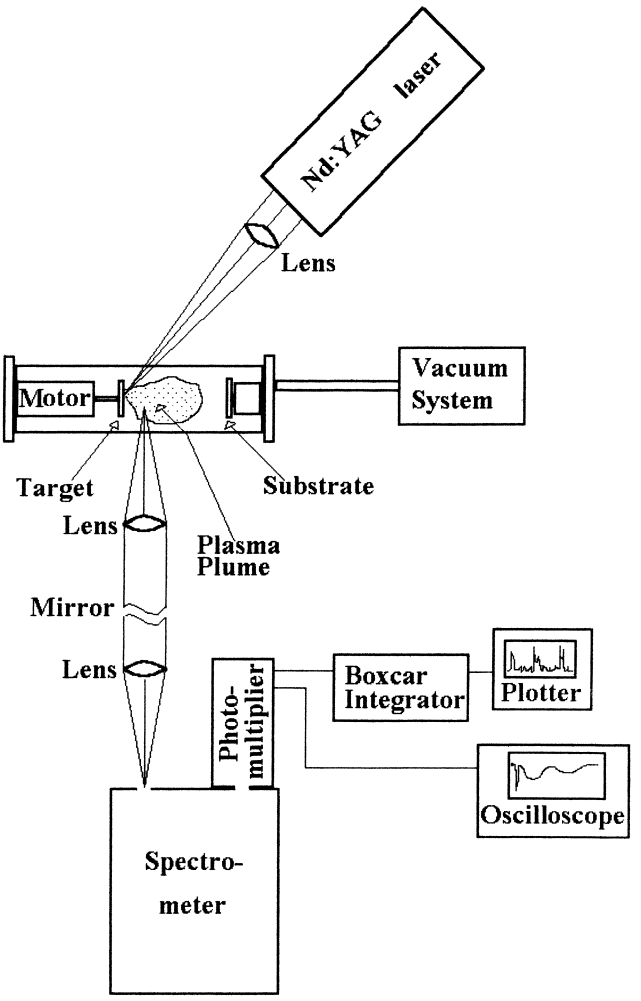

Fig. 1. Experimental set-up.

2. Experimental setup

The basic experimental set-up used for PLD consists of a vacuum chamber with a diffusion pump and an Nd:YAG laser (Lumonics HY 1200), set at the fundamental line ($\lambda = 1064$ nm) and at a repetition rate of 10 Hz to achieve the optimal output power. A pulse duration of 35 ns and an energy per pulse of 200 mJ are used. The laser beam is focused on the target surface with an approximately 15 cm focal length lens. Considering the focal length, the wavelength, the diameter and the spatial structure of the beam, a spot size of 0.36 mm in diameter is calculated. Subtracting loses, energy density on the target results of 80 J cm^{-2} and a power density of about 10^9 W cm^{-2}, enough to generate ionisation [14] and a luminous plasma. The laser radiation is introduced at 45° with respect to the target surface (Fig. 1). Pressure in the vacuum chamber is around 10^{-4} Torr. Pieces of pyrolytic graphite are used as targets. The substrates are silicon wafers previously cleaned with alcohol and acetone. A target-to-substrate distance of about 4 cm and a deposition time of 15 min yield film thicknesses of about 1 μm.

The light emitted from a selected spatial region of the laser induced plasma, chosen within 0 to 9 mm from the target surface, is collected by a lens ($f = 7$ cm), placed and centred at the focal distance. The resulting parallel beam is fed into a 0.01 nm resolution Czerny–Turner spectrometer through a second lens ($f = 40$ cm) focused at the entrance slit. Slit aperture and lenses yield a spatial resolution of about 2×10^{-2} mm^3. The signal is detected with a photomultiplier and fed into a boxcar integrator and plotter.

For the time-resolved measurements the spectrometer is tuned to a selected wavelength, and the signal from the photomultiplier is then fed into an oscilloscope. The oscilloscope or the boxcar electronic system is triggered by a reference signal coming from the Pockells cell of the laser cavity Q switch.

Substrate temperature is controlled using a coaxial

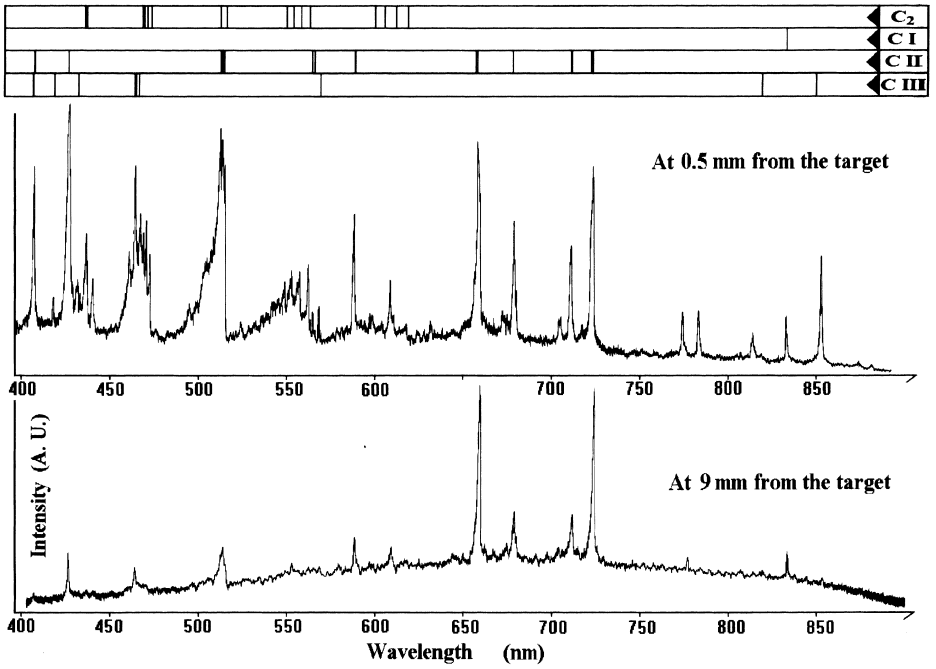

Fig. 2. Emission spectra of the plasma at 0.5 and 9 mm from the target surface, with 80 J cm^{-2} laser energy density per pulse. Intense tabulated lines for CI, CII, CIII and strong bands for C_2 are shown above. The intensity scale is different for each spectrum.

resistance and measured with a chromel–alumel thermocouple.

Raman spectroscopy measurements are performed at room temperature, in an air environment, with a Jobin Yvon U1000 double monochromator using the 514.5 nm line of an argon laser at a power level of 100 mW. The signal is detected with a photomultiplier and a standard photon counting system.

3. Results

3.1. Studies of the plume

3.1.1. Time-integrated measurements

The optical emission spectra of the plume consist of discrete peaks over a continuous broad background. The spectra obtained at 0.5 and 9 mm from the target are shown in Fig. 2. Most of the intense peaks are related to neutral, singly ionised and doubly ionised, atomic carbon [15]. The emission peaks are actually broadened lines, Stark and Doppler broadening being the main mechanisms responsible for the observed widths. The strong bands are due to the $\Delta v = -2, -1, 0, +1, +2$ vibrational sequences (Swan system) of the C_2 molecule $A^3\Pi_g$–$X'^3\Pi_u$ electronic transition [16]. Some peaks could not be identified with tabulated lines for carbon. The continuous background is mostly the result of Bremsstrahlung emission, radiation arising from accelerating free charged particles, but free-to-bound electron transitions (recombination) also contribute. At 0.5 mm from the target, this 'white' emission maximum is centred at short wavelengths ($\sim$400 nm). The continuous background emission may be fitted to an approximately 7350 K black body radiation spectrum. The intensity of the whole emission decreases as the distance from the target is increased and the white emission's maximum shifts to longer wavelengths, indicating plasma cooling. At 9 mm from the target the computed temperature falls to approximately 4300 K.

3.1.2. Time-resolved measurements

The evolution in time of three atomic emission lines is studied. Each line belongs to a different emitting species: CI ($\lambda = 833.5$ nm) to neutral atomic carbon, CII ($\lambda = 723.6$ nm) to singly ionised atomic carbon, and CIII

Table 1
Energy levels of three emission lines present in the plume, the transitions involved and the lifetimes quoted from Refs. [17–19]

Species	Wavelength (nm)	Energies of lower and upper levels (cm^{-1})	Transition	Lifetime (ns)
C I	833.51	61982–73976	3s $^1P_1^\circ$–3p $^1S_0$	31.25
C II	723.64	131736–145551	3p $^2P_{3/2}^\circ$–3d $^2D_{5/2}$	22.7
C III	464.74	238212–259724	3s $^3S_1$–3p $^3P_2^\circ$	13.7

($\lambda = 464.7$ nm) to doubly ionised atomic carbon. Table 1 presents other relevant data regarding these atomic lines. The light detected at various distances along the plume symmetry axis is viewed in an oscilloscope. Photographs of this signal are taken and then digitized. The result is shown in Figs. 3–5. Notice that the emission of most of the observed atomic transitions is present for much longer times than their corresponding lifetimes; this is due to re-excitation within the plasma plume [10]. Interpretation of these oscillographs is based on the assumption that the excited particle density is proportional to its emission intensity.

There are two clear maxima in all the graphs of Fig. 3. The first one at about 25 ns and measured at 0.5 mm from the target is very strong. This peak is present in the spectral range 400–900 nm so it must be a part of Bremsstrahlung emission. It also appears very early, independently of the distance to the target, which leads us to consider that generalised excitation due to fast electrons is responsible for most of the broad band continuous background. The second maximum is actually the characteristic CI ($\lambda = 833.5$ nm) line. This peak shifts slightly toward longer time as distance to the target increases. The time at which this maximum is recorded can be related with the time at which most of the emitting CI atoms go through the observation point. In this way, the time delay as a function of the distance

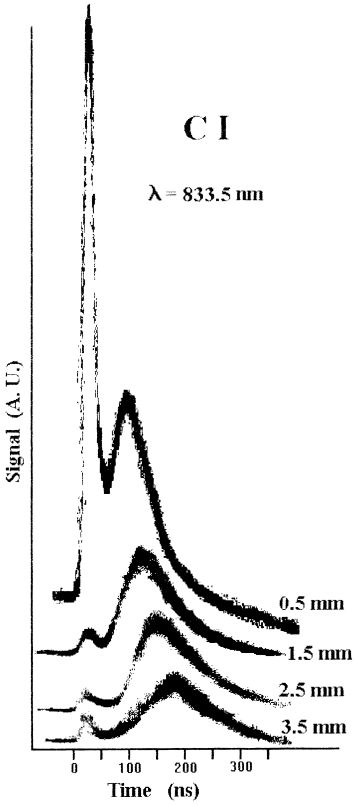

Fig. 3. Oscilloscope graphs of the CI (neutral carbon atom) $\lambda = 833.5$ nm emission line as a function of time, at distances of 0.5, 1.5, 2.5 and 3.5 mm from the target surface. Although the signal is in arbitrary units, the scale is the same for a better comparison between graphs.

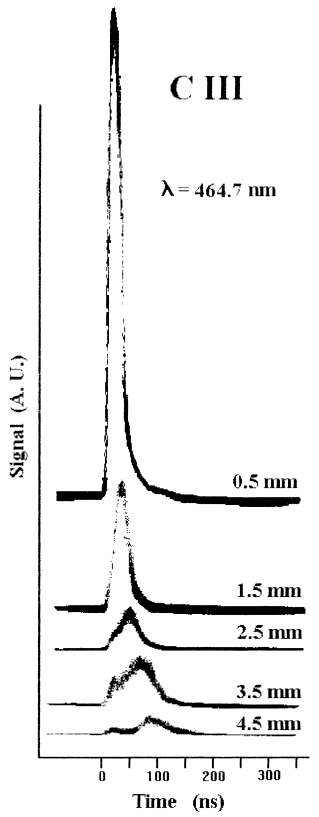

Fig. 4. Oscilloscope graphs of the (doubly ionised carbon atom) CIII $\lambda = 464.7$ nm emission line as a function of time, at 0.5, 1.5, 2.5, 3.5 and 4.5 mm from the target surface. Although the signal is in arbitrary units, the scale is the same for a better comparison between graphs.

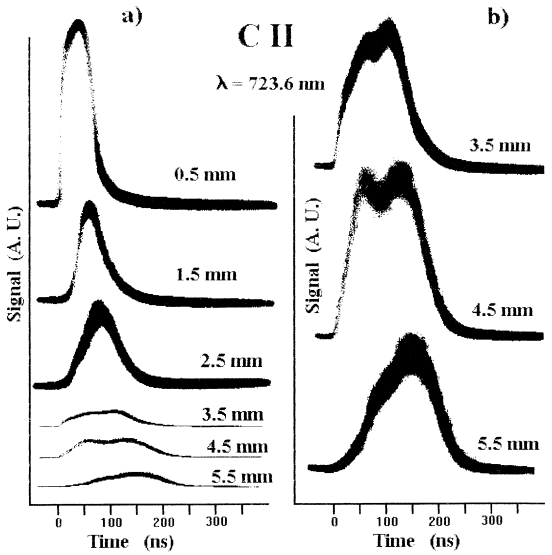

Fig. 5. Oscilloscope graphs of the (singly ionised carbon atom) CII $\lambda = 723.6$ nm emission line as a function of time, at 0.5, 1.5, 2.5, 3.5, 4.5 and 5.5 mm from the target surface. (a) shows all the graphs whereas (b) is an amplified version of the graphs at greater distances.

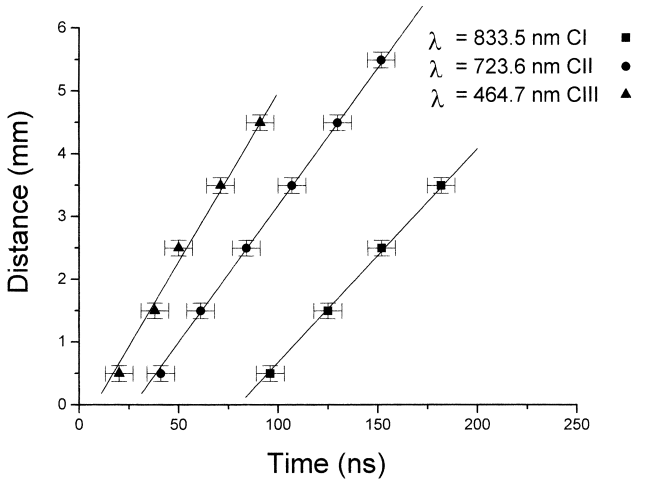

Fig. 6. Plot of the time at which the maxima appear for the various distances from the target surface. The resolution width is shown. The velocities obtained from the slopes are as follows: CI, 34 ± 2 km s^{-1}; CII, 44 ± 2 km s^{-1}; CIII, 54 ± 4 km s^{-1}.

to the target allows us to compute mean velocities for the components of the expanding plume. Fig. 6 presents this information for the three species studied.

Fig. 4 exhibits the evolution in time for the CIII ($\lambda=$ 464.7 nm) emission line. It looks very similar to Fig. 3, except that the characteristic emission appears earlier, sharper and stronger, overshadowing the Bremsstrahlung peak on the measurements at a distance lower than 3 mm from the target.

Fig. 5 shows the CII ($\lambda=723.6$ nm) line evolution. At distances greater than 3 mm from the target, two distinct maxima may be observed, but both are mostly characteristic CII emission. The light emitted at this wavelength is very intense and hides the relatively dimmer white Bremsstrahlung peak. The left maximum that appears at about 60 ns may be a consequence of recombination events between faster CIII ions and electrons leading to the formation of CII ions, which then decay through the 723.6 nm transition

By examining Fig. 6, we see that more highly ionised atoms travel faster. Calculated velocities of 34 ± 2 km s^{-1} for CI, 44 ± 2 km s^{-1} for CII, and 54 ± 4 km s^{-1} for CIII, corresponding to energies of 72, 120 and 181 eV respectively, show how the distribution of excited species varies with the distance from the target. At a given time, the more ionised species travel in front of the others. The neutral population behaviour is close to that expected for an unsteady adiabatic expansion. The transfer of thermal energy to kinetic energy during a type of unsteady adiabatic expansion into vacuum called 'outflow' [20,21], is predicted to result in velocities v of the expansion front:

$$v=\left(\frac{2}{\gamma-1}\right)\left(\frac{\gamma kT}{m}\right)^{1/2} \quad (1)$$

where γ is the ratio of specific heats C_p/C_v, k the Boltzmann constant, m the atomic mass and T the initial temperature [10,20–23]. Taking $\gamma=1.2$, which is an approximate value for the specific heat ratio accounting for ionisation and dissociation [22,23], $T=7\,350$ K and the carbon atomic mass number 12, velocities of about 25 km s^{-1} are calculated. This is close enough to the experimental results for neutrals, the difference can be attributed to the computed temperature, since only the continuous background is taken in to account. But most likely it is because the outflow model is thought for an ideal gas with a constant γ, which is an oversimplification of the conditions.

The relation among the calculated species velocities is consistent with he following qualitative description. At power densities of about 10^9 W cm^{-2} the surface heating is mostly indirect resulting from the quenching of hot carriers in the bulk (electrons) [24]. The electrons leave the target surface more easily and they move faster than ions or neutral species. However, because of the strong space charge field arising from the escaping electrons, they remain near the dense plasma. The Coulomb attraction of the ions and electrons, which nearly escape from the plume boundary, produces a space field that tends to accelerate ions according to their charge [10].

3.2. Raman spectroscopy of the films

Raman spectroscopy has been widely used in characterising diamond-like thin films obtained by various methods [5,9,11–13,25]. Diamond has a single Raman-active first-order phonon mode, which appears as a sharp line at 1332 cm^{-1}. Also graphite has only one high-frequency first-order Raman line at 1580 cm^{-1}. The line is referred to as the G band, and has been assigned to a stretching mode C–C within individual graphite sheets [11]. The C–C bonding that makes up the individual graphite layers is very strong as opposed to the inter-layer bonding which is weak. The stacking sequence is easily disordered while the carbon hexagons that make up the individual sheets are very stable [11]. This means that the G band, although broadened and/or shifted, must be clearly seen even in disordered graphite, i.e. even in a rather amorphous carbon that has enough sp^2 bonds. In well-crystallised graphites with small particle size, the D band appears at lower wave numbers, around 1357 cm^{-1} [5,11,12]. The small size of polycrystalline graphites causes a breakdown of a Raman scattering selection rule for larger crystals, allowing another phonon to contribute to the Raman scattering [11]. An obstacle to interpretation may be the spectral overlapping of the diamond line with the D band. A Raman spectrum of the pyrolytic graphite target showing G and D features is presented in Fig.7.

It is known that ablating a graphite target, with power densities varying between 10^8 and 10^{11} W cm^{-2},

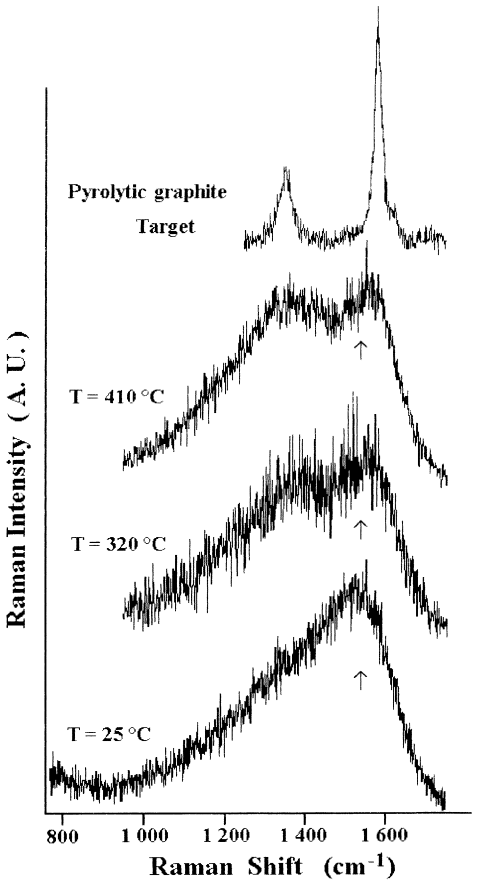

Fig. 7. Raman spectra of the pyrolytic graphite target and the film samples, grown at different substrate temperatures. The arrow marks 1540 cm^{-1}.

results in diamond-like amorphous films [4–7,12]. These films contain sp^2 (graphite) and sp^3 (diamond) bonding types. Raman spectra of the grown films are shown in Fig. 7; they are similar to other reported diamond-like films Raman spectra deposited under analogous conditions [5,12]. The D band appears at about 320°C and grows as the substrate temperature increases. The G band is always present; it is shifted towards lower wavelengths and broadened with decreasing substrate temperature. The shift of the graphite G band towards lower frequencies is related to the lengthening of the C–C intra-layer sp^2 bonds [13]. As this distance increases some atoms may leave the layer and under these conditions inter-layer sp^3 bonds become probable. This band shifting towards lower wave numbers (1540 ± 20 cm^{-1}) is considered by some authors as a signal of a new structure: 'bridged graphite', explaining the properties of diamond-like materials [13]. Other researchers have found that this shifted G band also appears in ion-damaged crystalline diamond [25].

3.3. Optical micrographs

One of the main disadvantages of PLD is the 'splashing' effect [2], which spoils the film surface quality. In this case, micrographs show that the surface quality is fairly good; no serious splashing is present. Fig. 8 presents two micrographs: (a) shows the surface of a film

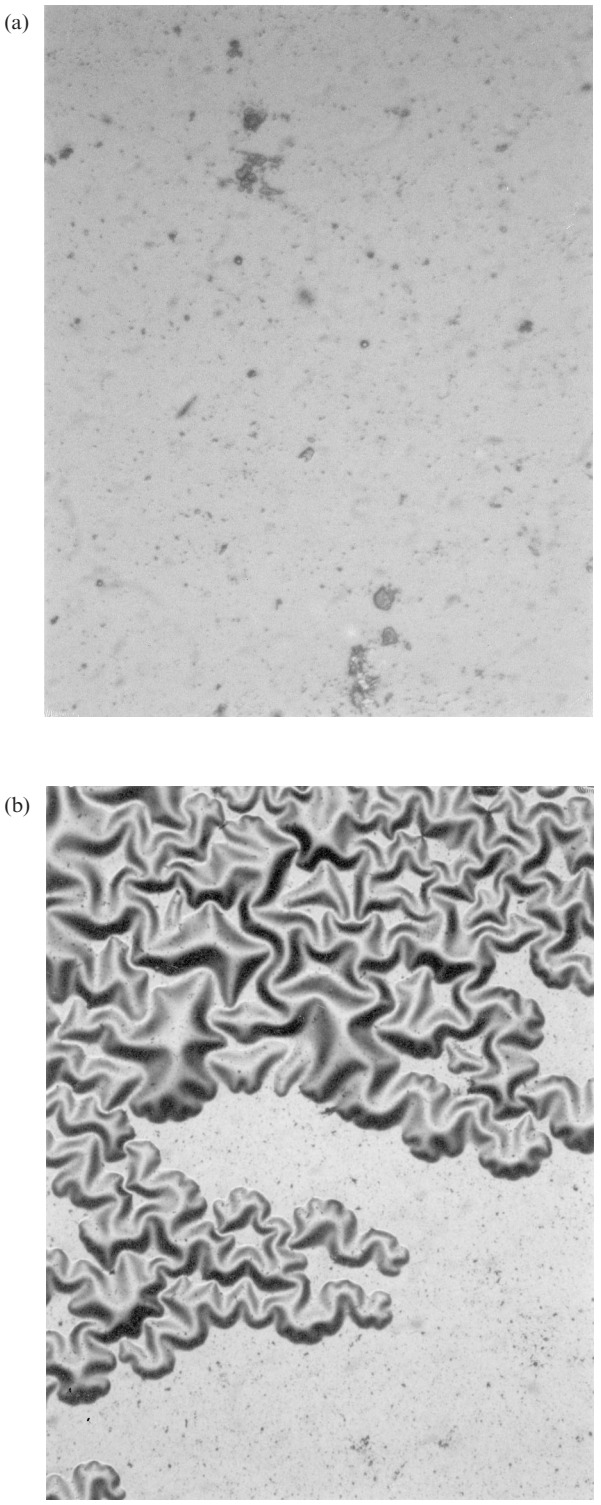

Fig. 8. Optical micrographs of the film surface. (a) (original magnification, 40×) exhibits a fairly smooth film surface, grown at 410°C. (b) (original magnification, 10×) shows how a film, grown at room temperature, curls up and peels off the substrate.

grown at 410°C; (b) shows a sector of a film, grown at ambient temperature, which is detaching from the substrate. At higher growth temperatures adhesion to the substrate is stronger. The films that stick better to the substrate have a more graphitic character. Adhesion depends on the matching of substrate material with the film, surface tension, previous cleaning and the energies of the first ablation species arriving to the substrate, which may form an interface [6,7]. Better diamond-like films present greater surface tension and detach more easily.

4. Discussion and conclusions

Optical emission spectroscopy is a powerful and non-destructive method to obtain information about PLD plasma dynamics. This technique revealed fast neutral and ionised atomic species within the plasma plume. The spatial distribution is different for each species: the more ionised species travel ahead and faster than the neutrals. This result is explained by Coulomb boosting at the early stages of the expansion. The white Bremsstrahlung emission reaches a maximum very early after the laser pulse, this leads us to consider that generalised excitation due the fast electrons is responsible for most of the broad band continuous background. Electron–ion recombination may account for the characteristic double peak during time-resolved measurements of the CII ($\lambda = 723.6$ nm) line.

The substrate temperature seems to play a role in the structure of diamond-like films. At room temperature, the broadened and shifted G band reveals highly disordered carbon with stretched sp^2 and some sp^3 bonds. As the substrate temperature increases, the G band appears less broadened and closer to 1580 cm^{-1}, indicating that sp^2 bonds are returning to their normal length along with a decrease of sp^3 bonds. Small graphite crystals are formed giving rise to the D band. So, with higher substrate temperatures, films grow more graphitic-like in character. The material deposited on substrates at room temperature is amorphous; sp^3 and sp^2 bonds are present. When the substrate is heated, graphitic order builds.

Graphite is the stable phase for elemental carbon under normal situations. Conditions such as extremely high pressures are needed to obtain sp^3 bonds. Quenching a large amount of highly energetic plasma species on a cold substrate, leaving no time or external thermal energy for a stable order to build, may favour an amorphous structure and the formation of sp^3 bonds. Some authors consider that for depositing carbon species to form sp^3 bonds, the species must grow in a state of very high local pressure. This pressure can be achieved through the creation of point defects from ion implantation into a sub-layer just below the deposition surface [9]. In any case high energy carbon atoms would be required. The atomic kinetic energies reached with 80 J cm^{-2}, provided by the present Nd:YAG laser, are similar to the kinetic energies reported in other works [7,8] produced with lower laser energies, under excimer laser excitation and with similar pulse duration. This higher efficiency for smaller wavelengths is explained if the light penetration depth is shorter, even when the total laser energy absorption is comparable. That way, higher temperatures may be reached closer to the surface, making larger kinetic energies possible. Assuming a linear response, the penetration depth ($1/\alpha$) for graphite at $\lambda = 1\,064$ nm is two to five times greater than that between 200 and 300 nm. However, owing to the high intensities we are dealing with, linear mechanisms are not enough to explain this together with other published results. For example, to attain similar plasma and film characteristics, an ArF laser ($\lambda = 193$ nm, $1/\alpha = 20$ nm) needs less than half the energy of a KrF laser ($\lambda = 248$ nm, $1/\alpha = 8$ nm) [8]. Other light absorption mechanisms must be playing an important role. At high laser intensities it is possible to take individual ions directly into anti-bonding states [20,26], and this effect enhances light absorption and phase transitions. At higher photon energies (shorter wavelengths), this fast transition should become more probable. Better absorption at the target surface may prevent the laser light from penetrating deeper, leading to less ablated material and yielding lower deposition rates. This may also explain why an earlier work [7] reports film thicknesses always under 600 nm with a KrF laser, the same deposition time, slightly smaller target-to-substrate distance and a wide range of energy densities (10–5000 J cm^{-2}).

Optical emission spectroscopy can be further used to measure quantities such as species velocities, helping to keep them constant while varying other parameters, such as laser wavelength or power, to determine the particular role that they play on the resulting film. These findings may finally reveal the actual physical mechanisms involved. The non-destructive character of optical emission spectroscopy may also be further exploited, and the plasma environment may be diagnosed in real time while growing a good quality film, providing information for precise parameter control.

Acknowledgements

The present work has been supported by Mexican 'Consejo Nacional de Ciencia y Tecnología (CONACYT)' under contract number 4225-E9405. The authors thank CONACYT and UAM for making the scientific exchange between our laboratories possible. They also thank Dr. Alessio Perrone from the University of Lecce, Italy, for his suggestions and comments.

References

[1] S.B. Ogale, A.P. Malshe, S.M. Kanetkar, Formation of diamond particulates by pulsed laser irradiation of graphite immersed in benzene, Solid State Commun. 84 (4) (1992) 371–373.

[2] T. Cheung Jeffery, History and fundamentals of pulsed laser deposition Chapter 1, in: D.B. Chrisey, G.K. Hubler (Eds.), Pulsed Laser Deposition of Thin Films, Wiley, New York, 1994, pp. 1–22.

[3] C.B. Collins, F. Davanloo, D.R. Jander, T.J. Lee, H. Park, J.H. You, Microstructure of amorphic diamond films, J. Appl. Phys. 69 (11) (1991) 7862–7870.

[4] C.B. Collins, F. Davanloo, T.J. Lee, J.H. You, H. Park, Amorphic diamond films produced by laser ablation, in: B. Braren, J.J. Dubowski, D.P. Norton (Eds.), Laser Ablation in Materials Processing: Fundamentals and Applications, Symposium Proceedings, Materials Research Society, Philadelphia, PA, 1992, pp. 547–562.

[5] S. Leppävuori, J. Levoska, J. Vaaray, O. Kusmartseva, Laser ablation deposition of diamond-like carbon films, in: B. Braren, J.J. Dubowski, D.P. Norton (Eds.), Laser Ablation in Materials Processing: Fundamentals and Applications, Symposium Proceedings, Materials Research Society, Philadelphia, PA, 1992, pp. 557–562.

[6] C.B. Collins, F. Davanloo, Noncrystalline carbon films with the bonding and properties of diamond Chapter 17, in: D.B. Chrisey, G.K. Hubler (Eds.), Pulsed Laser Deposition of Thin Films, Wiley, New York, 1994, pp. 417–430.

[7] C. Germain, C. Girault, J. Aubreton, A. Catherinot, S. Bec, A. Tonck, Photoablation of a graphite target by a KrF laser beam. Realisation of hard carbon thin films, Diamond Relat. Mater. 4 (1995) 309–313.

[8] A.A. Puretzky, D.B. Geohegan, G.E. Jellison Jr., M.M. McGibbon, Diagnostics of ArF- and KrF-laser generated carbon plumes used for amorphous daimond-like carbon film deposition, Appl. Surf. Sci. 96–98 (1996) 859–865.

[9] M.P. Siegal, L.J. Martínez-Miranda, N.J. Dinardo, D.R. Tallant, J.C. Barbour, P. Newcomer-Provencio, Characterization of amorphous carbon films grown by pulsed-laser deposition, Proceedings SPIE International Symposium on High Power Laser Ablation, 26–30 April 1998, Santa Fe, NM, to be published.

[10] D.B. Geohegan, Diagnostics and characteristics of laser-produced plasmas Chapter 5, in: D.B. Chrisey, G.K. Hubler (Eds.), Pulsed Laser Deposition of Thin Films, Wiley, New York, 1994, pp. 115–166.

[11] D.S. Knigth, W.B. White, Characterization of diamond films by Raman spectroscopy, J. Mater. Res. 4 (2) (1989) 385–393.

[12] M.A. Capano, F. Quian, R.K. Singh, N.T. McDevitt, Structural analysis of carbon thin films deposited by pulsed laser deposition, in: B. Braren, J.J. Dubowski, D.P. Norton (Eds.), Laser Ablation in Materials Processing: Fundamentals and Applications, Materials Research Society, Philadelphia, PA, 1992, pp. 569–574.

[13] P.V. Huong, Structural studies of diamond films and ultrahard materials by Raman and micro-Raman spectroscopies, Diamond Relat. Mater. 1 (1991) 33–41.

[14] P. Langer, G. Tonon, F. Floux, A. Ducaze, Laser induced emission of electrons, ions and X-rays from solid targets, IEEE J. Quantum Electron. QE-2 (9) (1966) 499–506.

[15] , in: R.C. Weast (Ed.), CRC Handbook of Chemistry and Physics, CRC Press, Boca Raton, FL, 1990, pp. E211–E332.

[16] R.W. Pearse, A.G. Gaydon, The Identification of Molecular Spectra, Wiley, New York, 1976.

[17] J. Reader, C. Corliss, W.L. Wiese, G.A. Martin, Wavelengths and Transitions Probabilities for Atoms and Atomic Ions, NSRDS, 1980, pp. 371–372.

[18] A.R. Striganov, N.S. Sventitskii, Tables of Lines of Neutral and Ionized Atoms, Plenum, New York, 1968, pp. 83–108.

[19] W.L. Wiese, M.W. Smith, B.M. Glennon, Atomic Transition Probabilities, NRDS-NNBS-4, 1966, pp. 30–48.

[20] R. Kelly, A. Miotello, Mechanisms of pulsed laser sputtering Chapter 3, in: D.B. Chrisey, G.K. Hubler (Eds.), Pulsed Laser Deposition of Thin Films, Wiley, New York, 1994, pp. 55–88.

[21] Comments on explosive laser sputtering, Appl. Surf. Sci. 96–98 (1996) 205–215.

[22] Y.B. Zel'dovich, Y.P. Raizer, Physics of Shock Waves and High-Temperature Hydrodynamic Phenomena, Academic Press, New York, 1966, pp. 101–106.

[23] Y.B. Zel'dovich, Y.P. Raizer, Physics of Shock Waves and High-Temperature Hydrodynamic Phenomena, Academic Press, New York, 1966, pp. 570–585.

[24] L. Wiedeman, H. Helvajian, Photodesorption dynamics in threshold-fluence UV laser induced surface-decomposition of $Bi_2Sr_2CaCu_2O_8$, in: B. Braren, J.J. Dubowski, D.P. Norton (Eds.), Laser Ablation in Materials Processing: Fundamentals and Applications, Symposium Proceedings, Materials Research Society, Philadelphia, PA, 1992, pp. 3–15.

[25] J.F. Morhange, R. Beserman, J.C. Bourgin, J.C. Brosious, Y.H. Lee, L.J. Cheng, J.W. Corbett, Techniques for studying ion implantation in diamond, in: S. Namba (Ed.), Ion Implantation in Semiconductors, Plenum, New York, 1975, pp. 457–461.

[26] J. Kissel, F.R. Krueger, Ion formation by impact of fast dust particles and comparison with related techniques, Appl. Phys. A 42 (1987) 69–85.